Science of the Total Environment 922 (2024) 171212

Contents lists available at ScienceDirect

Science of the Total Environment

journal homepage: www.elsevier.com/locate/scitotenv

Indoor radon risk mapping of the Canary Islands using a methodology for volcanic islands combining geological information and terrestrial gamma radiation data

C. Briones [a], J. Jubera [b], H. Alonso [c], J. Olaiz [b], J.T. Santana [b], N. Rodríguez-Brito [b], A.C. Arriola-Velásquez [c], N. Miquel [c], A. Tejera [c], P. Martel [c], E. González-Díaz [a], J.G. Rubiano [c,*]

[a] Dpto. de Técnicas y Proyectos en Ingeniería y Arquitectura de la Universidad de La Laguna, 38204, Canary Islands, Spain
[b] Servicio de Laboratorios y Calidad de la Construcción del Gobierno de Canarias, 38107, Canary Islands, Spain
[c] Dpto. de Física, Universidad de Las Palmas de Gran Canaria, 35017, Canary Islands, Spain

HIGHLIGHTS

- Radon risk maps applying a methodology developed for volcanic islands
- These maps combine lithostratigraphic information and terrestrial gamma radiation.
- Indoor radon measurements confirm the suitability of risk maps.
- Crossing risk maps with urban fabric allows evaluating the risk in the population.
- An estimation of effective annual dose for each risk area defined is provided.

GRAPHICAL ABSTRACT

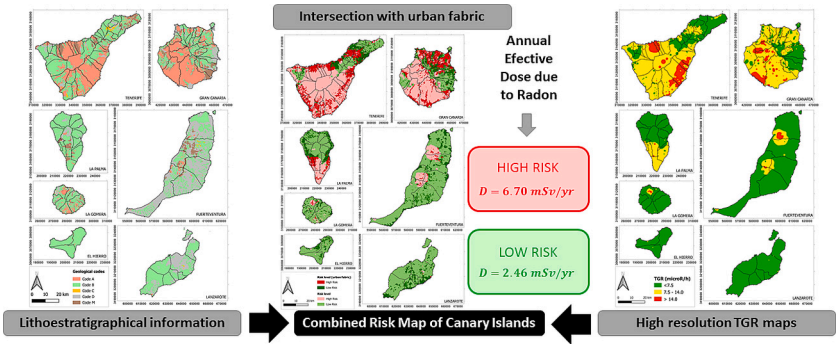

ARTICLE INFO

Editor: Pavlos Kassomenos

Keywords:
Indoor radon
Gamma radiation
Building codes
Risk maps
Radon dosimetry
Environmental radioactivity

ABSTRACT

Within the framework of the recent approval of the National Plan Against Radon by the Council of Ministers of the Spanish Government, one of its five axes focuses on the delimitation of priority action areas. In line with this objective, this paper presents the indoor radon risk maps of the Canary Islands. Due to the volcanic origin of the Canary Islands, there is a great deal of geological heterogeneity in the soils on which buildings settle, making it very difficult to delimit radon-risk areas in the process of creating maps. Following a methodology developed in previous works for a study area formed of a set of representative municipalities, this paper presents radon risk maps of the Canary Islands based on lithostratigraphic information and high-resolution terrestrial gamma radiation maps. The goodness of fit of these maps is verified based on a statistical analysis of indoor radon concentration measurements carried out at representative building enclosures. In order to analyse the level of risk to the population, these maps were combined with built up areas (urban fabric) maps and estimations of the annual effective doses due to radon was obtained by applying a dosimetric model. This methodology improves the capability to delimit indoor radon risk areas, with a greater margin of safety. In this respect, it is estimated that areas classified as low risk have indoor radon concentrations 41 % below the current reference level of 300 Bq/

* Corresponding author.
E-mail address: jesus.garciarubiano@ulpgc.es (J.G. Rubiano).

https://doi.org/10.1016/j.scitotenv.2024.171212
Received 24 November 2023; Received in revised form 6 February 2024; Accepted 21 February 2024
Available online 28 February 2024

m^3 established by national regulations in compliance with the precepts laid down in the European EURATOM Directive.

1. Introduction

Radon (^{222}Rn) is a noble gas arising from the decay chain of ^{238}U, which is present in certain proportions in soils and rocks and is the major source of the radiation dose received by humans (approximately 50 %). (UNSCEAR, 2000). This gas is capable of reaching the atmosphere, and is present in outdoor air in very low proportions; however, indoor spaces in buildings, and especially rooms on lower floors that are not properly ventilated, are susceptible to high concentrations of this gas. Its progeny in solid form, such as ^{218}Po, may be deposited and transported as aerosols and dust particles that are subsequently inhaled by the population; these particles then interact with lung tissue, thus increasing the risk of lung cancer, and are one of the main agents of this disease according to the World Health Organization (WHO) (World Health Organization, 2009). One of the methods used to quantify this health hazard is the application of dosimetry models representing exposure to a given concentration of radon activity, where both the unattached fraction and the equilibrium factor are taken into account (Cinelli et al., 2019).

For this reason, in recent years, countries have been introducing new regulations (or adapting their current legislation) with the aim of minimising the risk of exposure of their population to high concentrations of radon gas. At the European level, this legislation includes the 2013/59/EURATOM Directive of Basic Safety Standards (BSS) (Euratom, 2014) published by the European Commission. This directive calls on the governments of the Member States to adapt their legislation on the basis of the measures considered, and establishes that the reference level (RL) adopted cannot be higher than 300 Bq/m^3 for the annual indoor radon concentration (IRC). For this reason, Spanish regulations have incorporated a new section HS-6 within the Basic Document on Health Standards (DB-HS) of the Technical Building Code (Ministerio de Fomento, 2019), which applies to new construction and building refurbishment works, which reflect a RL of 300 Bq/m^3, complying with what is established by the European Commission. In addition, a new regulation on health protection against the risks arising from exposure to ionising radiation has recently been published (Ministerio de la Presidencia and R. con las C. y M.D, 2022), which sets out measures for the identification and anticipation of risks from exposure to ionising radiation, especially in the workplace. Both regulations, which share the objective of minimising the risk of exposure to high concentrations of radon, are supported by a current municipal risk map drawn up by the Spanish Nuclear Safety Council (CSN) (García-Talavera and López-Acevedo, 2019). The first National Radon Plan is currently in the process of being approved, and the activities carried out for its implementation include the refinement of radon risk maps by regional administrations.

Existing approaches to mapping indoor radon risk priority action areas are varied, and range from those based on measurements obtained from an intensive IRC measurement campaigns supported by geological information to obtain accurate and reliable maps (McColl et al., 2018; Miles et al., 2011). Also, there are maps based on methodologies involving the radioisotope content in rocks and soils (Ielsch et al., 2010), radon concentration in soil gas and permeability (Alonso et al., 2019; Pereira et al., 2017), or measurements of terrestrial gamma radiation (TGR) as a proxy variable strongly related to the content of^{226} Ra, the direct parent of ^{222}Rn (Arnedo et al., 2017; Briones et al., 2023; García-Talavera et al., 2013). Moreover, the scientific literature reports maps that combine IRC measurements with other variables such as geology information, radiological measurements and others for the identification of priority action areas (Cinelli et al., 2011; Fernández et al., 2021; García-Talavera and López-Acevedo, 2019).

It is important to consider the multifactorial nature of radon concentration levels inside building enclosures, where the lithological composition and permeability of the underlying soil are major factors (Font, 1997). However, there are other important factors, such as the construction materials used, the permeability of the foundation, the airtightness of the room, and extrinsic factors such as meteorological conditions (in particular, pressure variations), and the use and ventilation of the room (Collignan et al., 2016; Kropat et al., 2014; Zafrir et al., 2013).

The radon potential maps published by the CSN for mainland Spain (García-Talavera and López-Acevedo, 2019) were created using a methodology that combined data from the TGR (Quindós Poncela et al., 2004) with lithostratigraphic information. However, in the case of the Canary Islands, in order to obtain radon potential maps for use in risk zoning by municipal authorities to comply with current regulations, purely lithostratigraphic criteria were adopted (García-Talavera and López-Acevedo, 2019), due to the geological differences from mainland Spain and the availability of a higher density of radiological data from the islands. For the capital islands (Tenerife and Gran Canaria), the chemical composition of the rocks of the different lithostratigraphic units was considered (García-Talavera and López-Acevedo, 2019); this was used to *establish* a relationship between the alkaline mineral and silicate content with the help of a total alkali silica (TAS) diagram (Le Maitre, 2002) and the radioisotope content of the decay chain ^{238}U (Arnedo et al., 2017) to enable classification of the different areas. For the rest of the islands, a statistically sufficient number of IRC measurements were available, with values clearly below the RL, and these were therefore classified as non-priority action areas.

There are notable difficulties with the precise and reliable identification of radon risk areas in the Canary Islands, as a consequence of the geological heterogeneity characteristic of their soils due to their volcanic origin. Different types of lava flows, generally from different volcanic events and with clearly different compositions, are intermingled in small spaces, which can lead to radiological behaviour with great spatial variability. The methodology applied in this study was developed in previous work (Briones et al., 2023; Briones et al., 2021). This methodology is mainly based on intensive IRC and TGR measurement campaigns, and the processing of lithostratigraphic information on the geology of the Canary Islands. By combining all the available radiological and lithological information, and with the help of geographic information tools, combined risk maps can be drawn up to delimit radon-prone areas and contrast them with the available measured IRC data. In previous studies in which the methodology was developed, campaigns were carried out to measure other related variables such as the geogenic radon potential (GRP) as a function of the concentration of the radon activity in soil gas and its permeability, as well as the content of natural radioisotopes in soils by taking samples that were analysed using high-resolution gamma spectrometry (Briones et al., 2023). These campaigns allowed us to check the suitability of the combined risk maps obtained for the study areas with a representative geology of the soils of the archipelago, to verify that this methodology could be applied to the rest of the islands.

This article presents radon risk maps for the Canary Islands based on a methodology that includes an extension and intensification of the TGR and IRC measurement campaigns covering the whole archipelago. The percentage of buildings located in risk areas is then determined by combining these risk maps with the built up areas available in the urban fabric maps, and criteria are proposed for the establishment of a new risk zoning scheme for the Canary Islands. Finally, detailed data on the radon risk in the islands are used to obtain maps of the dose due to radon inhalation by applying a dosimetric model (García-Talavera and López-Acevedo, 2019; UNSCEAR, 2008).

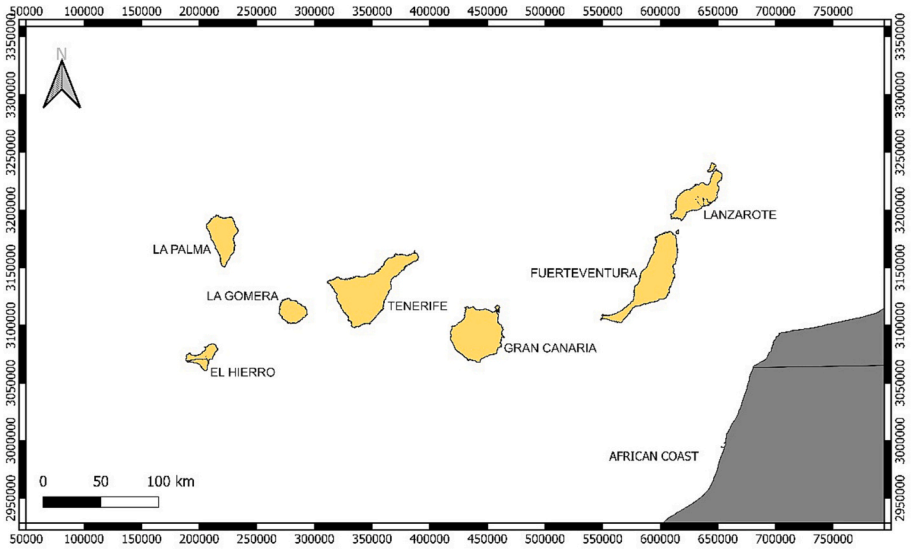

Fig. 1. Location of the Canary Islands.

2. Study area

The Canary Islands is an archipelago in the Atlantic Ocean, located approximately 100 km off the northwest coast of Africa and consisting of eight islands and five islets, with a distance of approximately 500 km between the easternmost and westernmost points of the archipelago (Fig. 1).

The islands are divided into two administrative provinces containing 88 municipalities, with a total surface area of 7492 km^2 and a total population of 2,223,951 inhabitants. The two main islands (with the largest surface area and population) are Tenerife and Gran Canaria. These islands have the largest population centres, with an average density of 506 inhabitants/km^2, and 82 % of the entire population of the Canary Islands live on these islands. Currently, all the municipalities of Tenerife and Gran Canaria are classified as priority action municipalities for radon risk, with the exception of two municipalities in the north of Tenerife (La Guancha and San Juan de La Rambla). The rest of the municipalities of the Canary islands fall outside of the radon risk classification (Ministerio de Fomento, 2019).

In the largest population centres, especially those located in metropolitan areas, high-rise buildings predominate (buildings with more than two floors), whereas the most common typology in the rest of the islands, and especially in rural areas, consists of single-family homes and buildings with one or two floors, accounting for approximately 88 % of the building stock in the archipelago (ISTAC, 2009). The protected natural space in the Canary Islands accounts for approximately 40 % of the total surface area of the archipelago, and the population centres in these areas are very small and normally of a rural nature. These areas include large expanses of natural parks, national parks, and reserves, which are almost depopulated, as they are usually steep and difficult to access.

3. Geological classification of the study area

The Canary Islands are of volcanic origin, with an approximate age of 30 million years. They include submarine and subaerial volcanic stages, with the eastern islands being the oldest and the western islands the youngest.

The volcanic rocks of the archipelago belong to the alkaline igneous series, and are related to intraplate volcanism (Carracedo et al., 2002). The most common rocks are basalts (undifferentiated terms), trachybasalts (intermediate) and phonolites and trachytes (differentiated).

The lithological map of the Canary Islands is characterised by a high degree of heterogeneity in relatively small areas, as a consequence of the intercalation of different geological events throughout the history of the formation of the islands. Resources that allow for a certain simplification of the geological map are therefore required to adapt it to the needs of this work. For this purpose, a simplified geological classification is drawn up based on codes that are assigned to the geochemical characteristics and radiological behaviour of the various classified lithologies that make up the lithological map of the Canary Islands. This scheme is based on the classification proposed by (Arnedo et al., 2017) for the eastern Canary Islands with the help of a TAS diagram, which is used in geochemistry for the classification of volcanic rocks according to the ratio between the alkaline mineral content (Na_2O and K_2O) and the silicate content (SiO_2) (Le Maitre, 2002). Furthermore, the correlation between the composition of volcanic rocks and their radiological activity needs to be taken into account, as basic or ultrabasic (mafic) rocks have a low concentration of unstable elements within their crystalline structure, meaning that a lower radioactivity can be inferred, whereas intermediate and acidic (felsic) rocks have higher concentrations of radioactive elements, which would explain the high radiological activity of these rocks (Arnedo, 2014). Since the differences observed between the radiological behaviour of rocks with different codes are independent of whether these are volcanic or plutonic rocks, they are treated together in this classification, despite the textural differences between them. Table 1 presents the simplified geological codes used for the Canary Islands.

Table 1
Simplified Geological Coding for different lithologies.

Code	Description	Lithologies
A	Intermediate and acidic (felsic) rocks	Phonolites, trachytes, trachybasalts, rhyolites, syenites, etc. (and deposits where material predominantly comes from these rocks)
B	Basic and ultrabasic (mafic) rocks	Basalts, Basanites, Tephrites, phonolitic tephrites, etc. (and deposits where material predominantly comes from these rocks)
C	Clay-type terrestrial sediments	Lake soils and sandy-clay soils
D	Deposits	Sands, deposits and debris of generally variable composition depending on the surrounding lithology without a clear predominance
M	Mixed	Lithologies combining igneous rocks of different geological code (A and B) without a clear predominance

Table 2
Summary geographical and geological information of the islands.

Island	Population (inh.)	Area considered	Area (km^2)	Percentage of area by geological code (%)				
				Code A	Code B	Code C	Code D	Code M
La Palma	84,855	Total area	708.32	0.94	89.30	0.00	5.91	3.85
		Built up area	65.45	0.09	89.27	0.00	5.35	5.29
El Hierro	11,777	Total area	268.71	0.18	99.48	0.23	0.11	0.00
		Built up area	12.47	0.00	99.60	0.08	0.32	0.00
La Gomera	22,293	Total area	369.8	7.50	83.45	0.00	5.96	3.09
		Built up area	12.75	9.88	64.24	0.00	14.27	11.61
Tenerife	954,303	Total area	2034.38	26.42	61.29	1.87	4.19	6.22
		Built up area	279.47	17.97	67.50	5.20	5.97	3.36
Gran Canaria	864,576	Total area	1560.1	36.95	45.85	0.00	9.59	7.34
		Built up area	207.09	18.94	54.39	0.00	18.51	8.10
Fuerteventura	124,769	Total area	1659.74	1.03	61.34	0.60	33.79	3.24
		Built up area	110.88	0.31	59.02	1.23	38.71	0.74
Lanzarote	161,378	Total area	874.99	0.07	77.96	0.36	21.60	0.00
		Built up area	77.58	0.00	86.39	0.06	13.55	0.00

3.1. El Hierro Island

El Hierro is the youngest island of the archipelago (1.12 Myr), and has a total area of 268.71 km^2. It has a characteristic truncated tetrahedral shape that arises from the convergence of three ranges of volcanic cones. Most of the island is covered by cinder cones and recent lavas, with a low development of erosional gullies. Large landslides are also characteristic, most notably the giant El Golfo collapse (Troll and Carracedo, 2016a).

With regard to the composition of the island's rocks, basic lithologies (code B) predominate over almost the entire surface (Table 2). As can be seen from Fig. 2, these are scattered small areas of acidic and clayey lithologies, and are in sparsely populated areas.

3.2. La Palma Island

La Palma is approximately 1.70 Myr old, and covers a total area of 708.32 km^2. It has an elongated shape, in a north-south direction, and is formed from the northern shield volcano and the southern volcanic ridge of Cumbre Vieja.

In general, volcanism on La Palma covers much of the Oceanic Island Basalt series, ranging from primitive basanites and basalts to highly evolved phonolites. The latter predominate at the summit and on the flanks of the Cumbre Vieja rift, where felsic eruptions show evidence of dome collapse and block and ash deposits (Troll and Carracedo, 2016b).

Currently, Cumbre Vieja is the site with the greatest volcanic activity in the archipelago. The eruption of the Tajogaite volcano took place here in 2021; since this eruption, new lava flows have formed with a subaerial surface area of approximately 48 ha and a composition evolving from tephrites to basanites (IGME, 2022). TGR and IRC measurements were taken at La Palma after the eruptive event.

A total of 89.3 % of the island is made up of lithologies classified as code B (Table 2); in contrast, acid lithologies (code A) account for only 0.9 % and mixed lithologies (code M) account for 3.8 %. These predominate in a dispersed way in Cumbre Vieja, and on the west side of the Caldera de Taburiente (Fig. 2).

3.3. La Gomera Island

La Gomera is an island with an age of 9.40 Myr and an approximate surface area of 369.80 km^2. It has a roughly circular shape, and one of its most notable characteristics is its high altitude (1487 masl) in relation to its small surface area. The scarcity of recent volcanic activity and high rainfall has allowed for intense erosion, which has formed deep ravines. The predominant rocks on the islands are basaltic, although there are a large number of trachytic and phonolitic lava dykes and domes, with the highest concentration in the central area of the island. The Vallehermoso stratovolcano should also be mentioned, as this is related to a northward collapse that led to volcanic activity generating a large number of phonolitic domes and eruptions (Troll and Carracedo, 2016c).

Of the island's surface, 83.5 % is made up of code B lithologies (Table 2) and only 6.3 % of acid lithologies (code A); the latter are especially concentrated in the municipality of Vallehermoso in the north of the island, and in scattered lava flows in the municipality of Alajeró in the south of the island (Fig. 2).

3.4. Tenerife Island

Tenerife, with an age of 11.90 Myr, is the island with the largest surface area and height in the archipelago (2034.38 km^2 and 3718 masl). This island occupies a central position, and represents an intermediate evolutionary stage of the archipelago. The overall shape of the island is a flat-topped truncated tetrahedron with a nested stratovolcano (Teide). Three rifts converge at this summit, in the northwest, northeast and south directions (Troll and Carracedo, 2016d).

As shown in Table 2, 61.3 % of the surface area of Tenerife is made up of lithologies classified as code B; these are mainly basaltic lava flows, which include the old massifs (Teno and Anaga) and younger lava flows. A total of 26.4 % of the surface area is classified as code A, and this includes the central area of the Cañadas del Teide, the northwest of the island, and a large part of the south of the island, with lava flows from the southwest to the southeast. It is worth noting that a large proportion of the clayey lithology classified as code C, which accounts for only 1.9 %, is concentrated in a relatively large area in the north-east of the island, covering the central part of the Metropolitan Area of Tenerife (Fig. 2).

3.5. Gran Canaria Island

Gran Canaria, with an age of 14.60 Myr, is an island with an approximately circular shape and an area of 1560.10 km^2. It is characterised by a system of ravines that start in the central area, where the point of maximum altitude is located (1949 masl), and are distributed radially, as a result of erosion processes. The main geomorphological features are related to the different volcanic processes, and divide the island into two roughly equal parts around a diagonal axis running northwest-southeast. This axis coincides with a Pliocene rift zone. The southwestern area is the older part, while the northeastern area originates in the Plio-Quaternary and is the younger part in which the most recent volcanism is concentrated (Troll and Carracedo, 2016e).

The surface area occupied by code B lithologies is 45.9 %, which makes Gran Canaria the island with the fewest basic types of lithology. Code A lithology clearly predominates on the west side of the axis, covering 37 % of the surface area; however, the main urban centres of the island are to the east of the axis, where codes B, D and M are intermingled with a certain proportion of code A (Fig. 2).

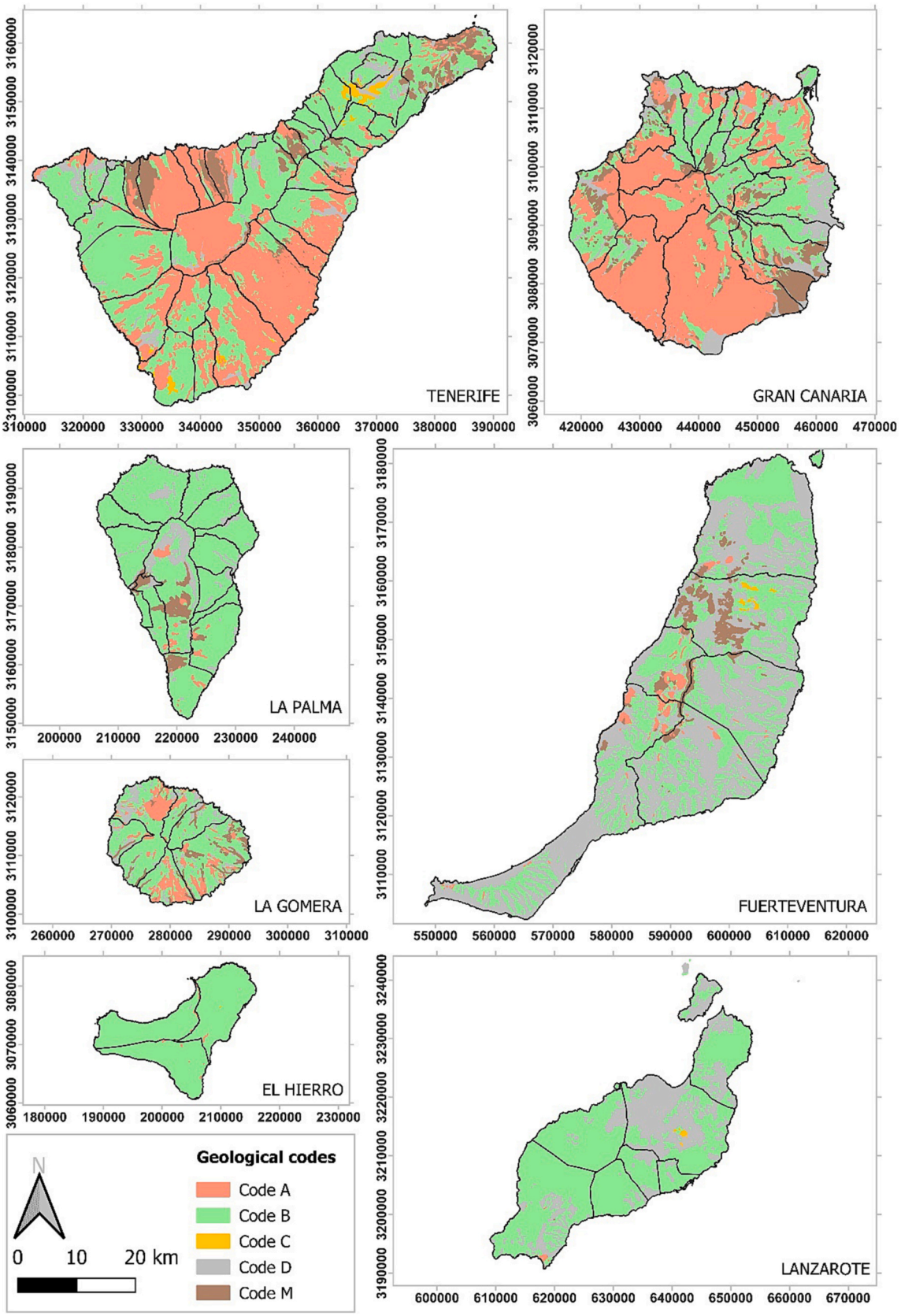

Fig. 2. Simplified geological code maps of the Canary Islands.

3.6. Fuerteventura Island

Fuerteventura, with an age of 20.20 Myr, has a total surface area of 1659.74 km^2 and a maximum altitude of 813 masl. Together with Lanzarote, this island forms a single continuous ridge from the El Banquete seamount in the south to the Chinijo archipelago in the north, parallel to the mainland coast of Africa. For a considerable period of time in its geological history, it was a single land mass with a length of 220 km. The main geomorphological features of Fuerteventura are the Jandía peninsula, which is joined to the rest of the island by an isthmus; the Betancuria massif, formed mainly of plutonic rocks that have resisted erosion to some degree; a 25 km long central plain; and the U-shaped eastern valleys.

As can be seen from Table 2, Fuerteventura consists mainly of alkaline basalts (code B) with a composition very similar to those originating from the most recent eruptions (Troll and Carracedo, 2016f). There is also a large proportion of deposits (code D) that are scattered throughout the island, with code A lithologies in the Betancuria (syenites and trachytes) and Tindaya (quartzotrachytes) areas (Fig. 2).

3.7. Lanzarote Island and La Graciosa Island

Lanzarote and La Graciosa are approximately 15 Myr old, and have a combined surface area of 875 km^2 and a maximum altitude of 670 masl. Like Fuerteventura, these islands have a geomorphology typical of mature islands, with a predominance of deeply eroded massifs, U-shaped ravines and high cliffs separated by a wide central plain covered with organic aeolian sands. The most recent volcanism (in the 17th and 18th centuries) is concentrated in the central rift zone of Lanzarote and in a northeast-southwest direction (Troll and Carracedo, 2016g).

As can be seen from Table 2, 99.6 % of the total surface area of the island is made up of basic lithologies (code B) and deposits (code D), with a small area of clayey lithologies (Code C) in the central-eastern part of the island (Fig. 2).

4. Materials and methods

4.1. Measurement campaigns

The campaigns carried out during this work have made it possible to incorporate a 41 % of new IRC data and 70 % of new TGR data with respect to previous campaigns (Alonso, 2015; Arnedo, 2014; Briones et al., 2023; Briones et al., 2021). Thus, a total density of 14 IRC data per 100 km^2 and 33 TGR data per 100 km^2 are available.

a) Indoor Radon Concentration (IRC) Measurement Campaign

Radosys RSKS detectors, which are based on a technique involving the detection of alpha particles, were used for the IRC measurement campaign. These detectors consist of a diffusion chamber housing a 100 mm^2 CR-39 chip. Their principle of operation relies on the decay process of ^{222}Rn to ^{218}Po, which results in the emission of alpha particles.

Radosys RSKS detectors have a typical equilibrium time of 3 h between the air sample and the surrounding environment, they offer remarkable sensitivity, registering 2.0 tracks•cm^2 •-kBq-1•h-1•m^3, and have a saturation capacity in excess of 12,000 kBqh/m^3. In terms of initial performance, they typically have a background of 0.3 tracks•mm^{-2}, and their detection limit is 6 Bq/m^3 over an exposure period of 90 days.

The development process for the detectors involved the use of a 25 %/6.25 M sodium hydroxide solution at a temperature of 90 °C, with a development time of 4.5 h. Two systems were used to process the dosimeters: NanoBath/NanoReader, and the 2000 System Radometer from Radosys. This equipment was available from the Laboratory and Construction Quality Service of the Department of Public Works and Transport of the Government of the Canary Islands on Tenerife Island, and from the Laboratory of Environmental Radioactivity of the Physics Department at the University of Las Palmas de Gran Canaria on Gran Canaria Island. We note that each battery of detectors was calibrated with specific parameters provided by the company, and was updated by means of reading software. In addition, periodic intercomparisons were carried out between the two laboratories and the results were compared with data from external certified laboratories, such as University of Cantabria (UC), to ensure the accuracy and quality of the measurements.

In this series of experiments, a total of 1064 IRC measurements sites were addressed in successive measurement campaigns across the study area, giving an average density of 14 data points/100 km^2, a density approximately six times higher than in the previous mapping of radon potential in Spain (García-Talavera and López-Acevedo, 2019). The spatial distribution of the measurements was designed to cover all geological codes with a sufficient number of samples per code which allows the application of statistical methods explained in Section 4.3.

These campaigns were carried out with the voluntary collaboration of the population via various dissemination channels, and in particular the press and social networks. Each participant was informed of the methodology and was provided with an application form, which made it possible to select appropriate applicants for the needs of this work. The selected dwellings and premises were required to have a representative building enclosure (RBE), i.e. a habitable building enclosure located on the floor closest to the ground, preferably on the ground floor (or the first floor if the ground floor was not possible), following the methodology defined in previous works by our team (Briones et al., 2021). This made it possible to homogenise the samples, which were also taken using the passive alpha track detectors described above; the measurements were not taken during the summer months (June to September), and were made over a minimum period of three months, in accordance with the conditions recommended by the CSN (Consejo de Seguridad Nuclear, 2012) and widely adopted by the scientific community (Elío et al., 2017). When data from previous campaigns were used, a curation of the measurements obtained was carried out so that they were taken in the RBE within the periods established in order to comply with the requirements of the methodology.

To guarantee the quality of the measurements, the detectors were placed and removed by members of our team, with duplicate detectors at each RBE, to ensure adequate height and separation from walls and other obstacles, and avoiding areas of draughts or heat sources. A protocol for the removal of the detectors was followed with the aim of minimising both the sample contamination and the time between the end of the exposure and the development and subsequent analysis of the detectors. For each measurement, relevant information was collected, such as the type of building, the type of enclosure, the living habits and the relevant construction characteristics.

In order to avoid possible distortions in the analysis of the results, the IRC values obtained from enclosures in dwellings with a ventilation chamber under the ground floor slab were discarded, since it was considered that a remediation solution was already available (Briones et al., 2021).

b) Terrestrial Gamma Radiation (TGR) Measurement Campaign

To carry out measurements of the TGR rate in the study area (a proxy variable for the identification of radon-prone areas), the Ludlum model 3019 was used as the main instrumentation. This radiometer is equipped with a high-sensitivity internal Csl scintillation detector, with a recording capacity of 175 cpm per μR/h. Its measurement range covers background gamma radiation levels up to 500 μSv/h or 50 μR/h.

The radiometer used for these measurements was calibrated in December 2020 by Ludlum Measurements, Inc., prior to the start of the measurement campaign in 2021.

Radiometers of this type are portable, and can be easily mounted on a tripod. This allowed them to be positioned at a constant a height of 1 m above ground level, thus ensuring homogeneity of the measurement conditions at different locations.

A total of 2450 TGR measurements were made in the different campaigns of this study, giving an average density of approximately 33 data points/100 km^2. This density is much higher than that used for the

elaboration of the Natural Gamma Radiation Map of Spain (MARNA) by the CSN for mainland Spain, where measurements were carried out with an average density of approximately 1.4 data points/100 km^2 (Quindós Poncela et al., 2004; Suárez-Mahou et al., 2000).

In order to guarantee an ideal distribution and correct delimitation of the areas with the highest TGR dose rate, especially in urban areas, a grid was drawn up for each island with cells of 3 × 3 km, and the rate of measurements per grid was established depending on the percentage of the surface area occupied by urban regions. A rate of 5–10 measurements was determined for grids with a larger built-up area, that is, a higher percentage of urban fabric, especially in metropolitan areas, and a rate of three measurements per grid was used in rural areas or areas with a lower building density. These rates were reduced for areas of protected natural space with little or no rural activity, with difficult accessibility, and where there were no buildings or urbanisation of the area was not possible.

When selecting the locations at which the TGR measurements were carried out, a list of conditions was considered in order to guarantee correct measurements. We chose land with the least possible disturbance, which had not been subjected to significant modifications, to ensure that it represented the natural terrain of the area as far as possible. The measurements were made in flat areas where possible, avoiding locations close to sloped walls, at the bottom of ravines, close to significant vegetation, or near water reservoirs, following the recommendations established by the CSN (Herranz et al., 2003). In more urbanised areas, measurements close to paved areas, walls, pavements (minimum distance 10 m), or any construction (minimum distance 15 m) were avoided. In built-up urban areas, where compliance with these conditions was difficult, measurements were taken in accessible plots that were as clear as possible, and were made in the central area, as far away as possible from artificial elements.

At each selected location, at least two natural gamma radiation dose rate measurements were taken with hand-held radiometers (as described above) at a height of 1 m above the ground, with a distance of approximately 10 m between them. In the event of obtaining a difference between the first two measurements of >10 %, a third measurement was made at a distance of 10 m from the first two, forming an approximately equilateral triangle. To characterise each measured location, the arithmetic mean (AM) of the values was taken, and the result was marked with the UTM coordinates of the approximate geometric centre of the measured points.

Measurements were always carried out between 8 am and 6 pm, avoiding rainy days and with a minimum gap of seven days since the last rainfall recorded in the area, in order to minimise the influence of high soil water content (Barbosa et al., 2018).

In order to obtain the natural gamma radiation rate arising exclusively from the radioisotopes present in the ground (TGR), the cosmic radiation background was subtracted from the direct measurements. The cosmic radiation background was estimated by means of the equation established by (UNSCEAR, 1993) as a function of the latitude and altitude above sea level; this was adapted for use in the Canary Islands by (Arnedo et al., 2017) as shown in Eq. (1):

$$\dot{D}(z) = 3.69\left[0.21e^{-1.65z} + 0.79e^{0.453z}\right] \quad (1)$$

where $\dot{D}(z)$ is the absorbed dose rate due to the cosmic background at the latitude of the Canary Islands (expressed in μR/h) and the altitude z (in km). In this equation, the value of 3.69 μR/h correspond to the exposure rate measured at sea level at the latitude of Canary Island (Arnedo, 2014), and the rest of constants were computed by (Bouville and Lowder, 1988) through an exponential fitting.

4.2. Statistical methods

Several statistical methods were used in this work for the definition of radon-prone areas; the approach used to calculate the statistical tolerance intervals used in previous works is worth mentioning (Briones et al., 2023; Briones et al., 2021), as this was used by the CSN for the preparation of "Cartography of the radon potential in Spain" (García-Talavera and López-Acevedo, 2019) and was developed by García-Talavera et al. (2013).

IRC measurements exhibit high levels of variability and skewness, which are characteristic of a dataset affected by random variables that follow a log-normal statistical distribution. In order to obtain the one-sided upper tolerance limit $\widetilde{X_p}$ with a confidence level of 100 (1 − α)% for 100p% of the population from which n data points are derived for a log-normal distribution is given by Eq. (2) (Odeh and Owen, 1980):

$$\widetilde{X_p} = X_g \cdot (S_g)^{g'_{(1-\alpha),p,n}} \quad (2)$$

where X_g is the geometric mean (GM), S_g is the geometric standard deviation (GSD), and $g'_{(1-\alpha),p,n}$ is a tabulated value (Meeker et al., 1991; Odeh and Owen, 1980) for different values of n, $(1-\alpha)$ and p.

In this work, to calculate the upper tolerance bound (UTB) of the sample groups, values of $\alpha = 0.10$ and $p = 0.90$ were used.

Finally, to prevent a type II error, a minimum number of samples $n \geq 27$ was considered, in line with the work of (García-Talavera et al., 2013). Above this number of IRC samples, the UTB is a reliable indicator, since above this limit, variations in n have little effect on the outcome (Briones et al., 2021).

4.3. Geoprocessing of results

To carry out a geostatistical analysis of the data and to generate the maps, the Quantum GIS (QGIS) geographic representation system was used. QGIS is a free, open source geographic information system (GIS) that is used in various fields, and is valuable in terms of the spatial management of the results obtained, the identification of anomalous behaviour, etc.

This tool was used to generate the different geological, radiometric and risk maps of the islands. To develop the simplified geological code maps, we used lithostratigraphic maps obtained from the Digital Cartography of the Geological and Continuous Map of Spain (GEODE), provided by the Geological and Mining Institute of Spain (IGME, 2021).

4.4. Calculation of effective dose from Indoor Radon Concentration (IRC)

To estimate the annual effective dose from exposure to a certain activity concentration of ^{222}Rn, dosimetric models must be used that consider the interaction between radon (and its progeny) and living tissue. From these dosimetric models, dose coefficients are derived that allow the radon inhalation dose to be calculated by multiplying the average radon concentration by the elapsed time and the corresponding dose coefficient, as shown in Eq. (3) (Cinelli et al., 2019; ICRP, 2010):

$$D = DC \cdot EEC \cdot t \quad (3)$$

where DC is the dose coefficient (in $Sv \cdot m^3 \cdot Bq_{EEC}^{-1} \cdot h^{-1}$). EEC is the equivalent equilibrium concentration of radon progeny, defined by

$$EEC\left(Bq_{EEC} \cdot m^3\right) = IRC\left(Bq \cdot m^{-3}\right) \cdot F \quad (4)$$

where F is the equilibrium factor between the free and bound fraction of radon progeny in air, and t is the exposure time. Unless there is evidence to the contrary, the International Commission on Radiological Protection (ICRP) recommends an equilibrium factor of F = 0.4 for both dwellings and workplaces (ICRP, 2014). Applying this balancing factor gives a recommended dose coefficient of 6.9 $nSv \cdot m^3 \cdot Bq_{EEC}^{-1} \cdot h^{-1}$ for most situations (ICRP, 2014).

Table 3
Terrestrial Gamma radiation (TGR) ranges and corresponding indoor radon concentration (IRC) expressed in terms of geometric mean (GM) (García-Talavera and López-Acevedo, 2019).

Potential exposure	TGR (μR/h)	IRC (GM)
Low	< 7.5	< 70 Bq/m^3
Medium	7.5–14.0	70–120 Bq/m^3
High	> 14.0	> 120 Bq/m^3

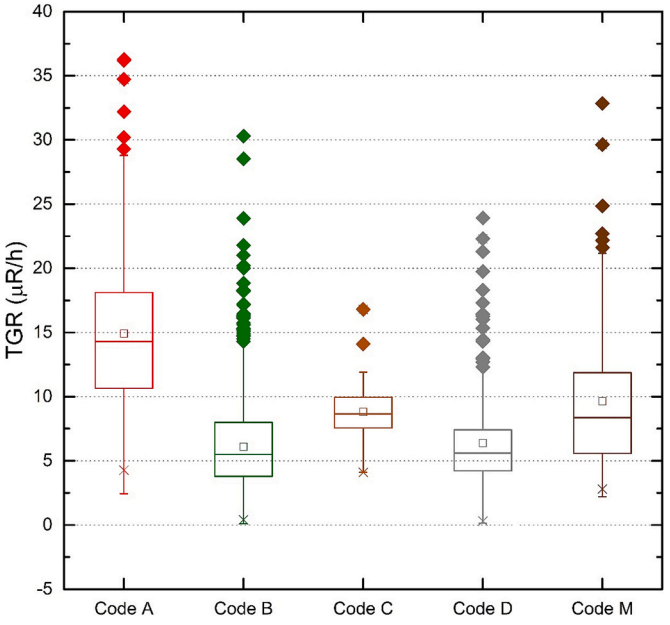

Fig. 3. Terrestrial gamma radiation (TGR) data distributed by simplified geological codes.

5. Analysis, results and discussion

This section first presents a comparison of the IRC and TGR data as a function of the geology, and then analyses the IRC data as a function of TGR, taking into account the limits established by the CSN (García-Talavera and López-Acevedo, 2019), as presented in Table 3. These ranges were previously used for the development of the methodology, since the results obtained for the Canary Islands were very similar to those obtained by the CSN for the rest of the Spanish territory (Briones et al., 2023).

The data are then analysed using risk maps of the study area based solely on geological information, and then using risk maps based solely on TGR. Next, risk maps combining geological and TGR information are proposed; their suitability is analysed, and the risk zones are combined with the urban fabric maps to allow for more accurate assessments of the radon risk to the population. Finally, the annual effective doses that the population would experience in the combined risk zone are estimated.

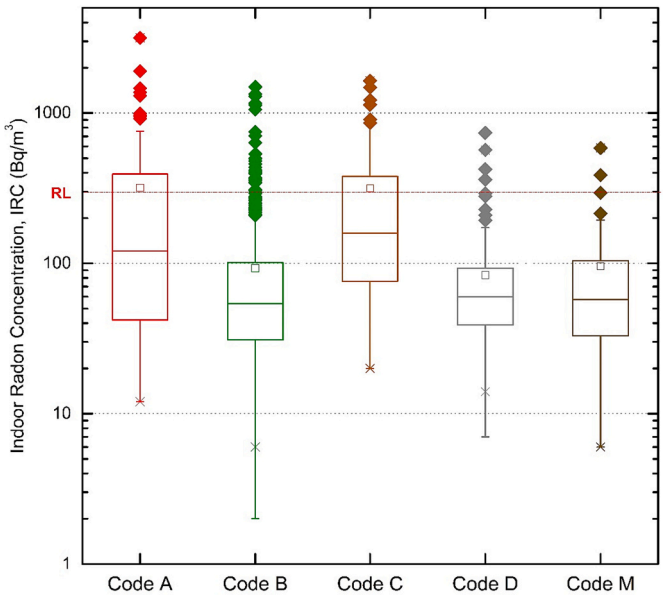

Fig. 4. Indoor Radon Concentration (IRC) data distributed by simplified geological codes.

Table 5
Statistical comparison of indoor radon concentration (IRC) results based on geological codes.

	Code A	Code B	Code C	Code D	Code M
n	83	721	59	159	42
GM (Bq/m^3)	134.3	56.4	180.2	62.2	59.9
GSD (Bq/m^3)	3.9	2.6	2.9	2.1	2.6
UTB (Bq/m^3)	**1021**	**207**	**934**	**177**	**281**
P90 (Bq/m^3)	887	174	829	138	194

5.1. Geology-based data analysis

We took the geological characteristics of the terrain in which the buildings were located as a priority factor influencing the levels of radon activity concentration inside the buildings, and used the available lithostratigraphic information as a proxy variable when creating risk maps (Hughes et al., 2022; Tondeur and Cinelli, 2014). To carry out this analysis, as described in Section 3, a simplified classification of the different lithologies into geological codes was used. In this section, we present an analysis of the TGR values measured experimentally according to the simplified geological code corresponding to the location of each measurement. Also, the IRC results measured in the RBE of each building considered were analysed according to the corresponding simplified geological code. Fig. 3 shows a box and whiskers diagram, from which a clear difference in the behaviour of code A can be observed with respect to the rest of the codes. We obtained a geometric mean of 13.7 μR/h (close to 14 μR/h), which was confirmed with a Bonferroni Post Hoc Test of Kruskal-Wallis comparing in pairs of code A with the rest of the codes ($p-value = 0.00 < 0.05$). Significantly different behaviour can also be observed for codes C and M (clays and mixed

Table 4
Statistical comparison of terrestrial gamma radiation (TGR) results based on geological codes.

	Code A	Code B	Code C	Code D	Code M
Number of simples, n	387	1592	44	279	148
Arithmetic mean, AM (μR/h)	14.9	6.1	8.8	6.4	9.6
Standard deviation, SD (μR/h)	5.9	3.4	2.3	3.9	5.4
Geometric mean, GM (μR/h)	**13.7**	**5.1**	**8.5**	**5.3**	**8.4**
Geometric standard deviation, GSD (μR/h)	1.5	1.9	1.3	2.0	1.7

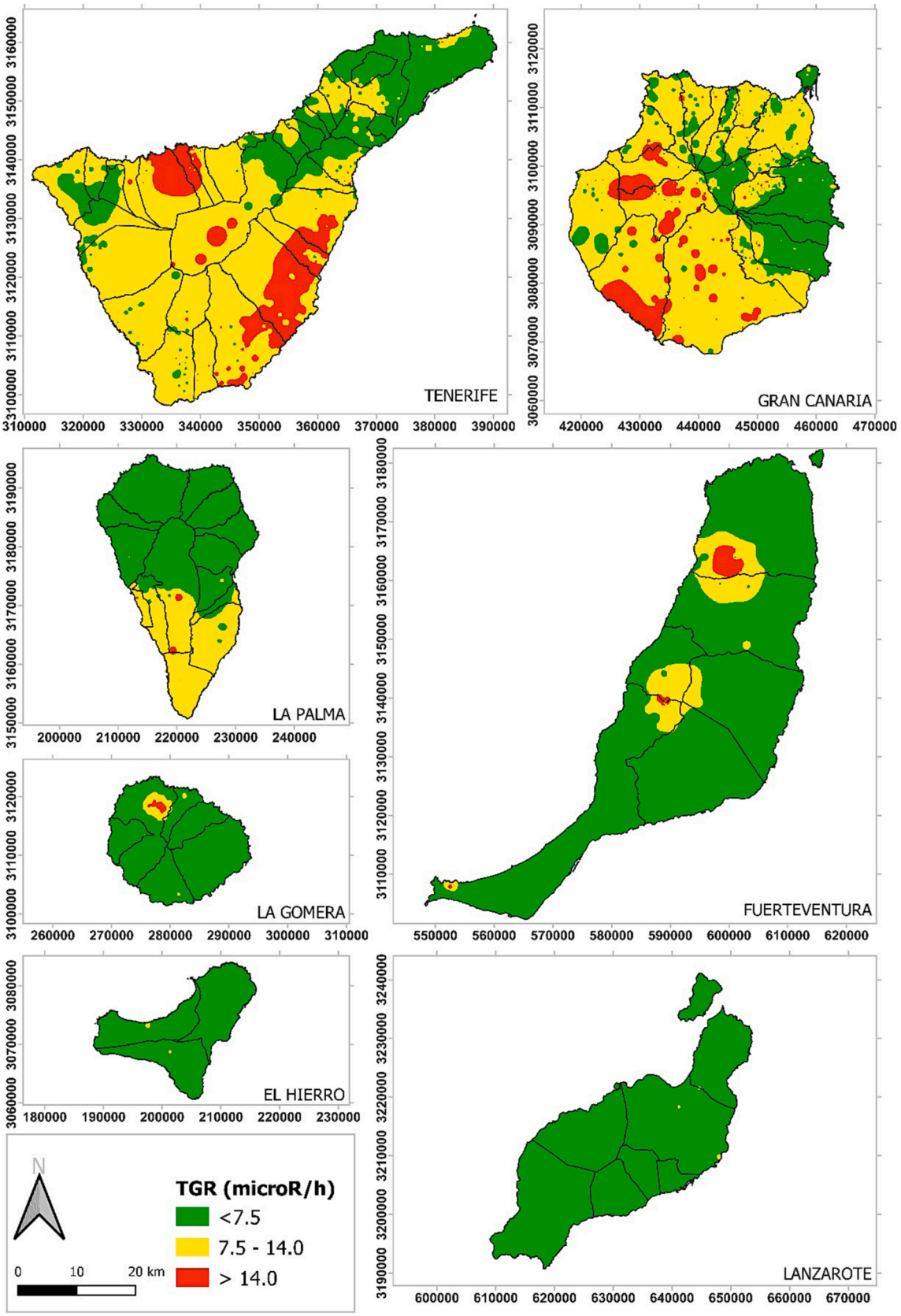

Fig. 5. Terrestrial Gamma Radiation (TGR) interpolated maps of Canary Islands.

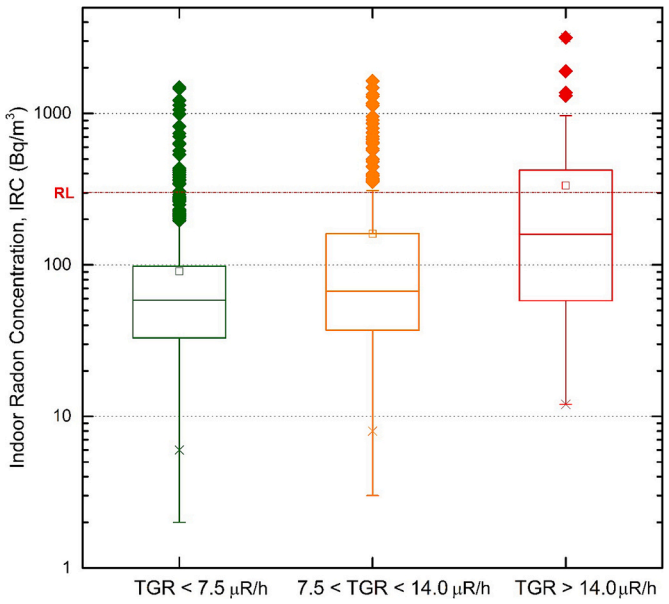

Fig. 6. Indoor Radon Concentration (IRC) data distributed by ranges of Terrestrial Gamma Radiation (TGR) ranges stablished by the CSN.

rocks), which both have a geometric mean above the classification level of 7.5 μR/h, with respect to codes B and D (basic and deposits), for which the geometric means of the measurements correspond to the low radon risk range (< 7.5 μR/h) (Table 4). Significant differences in the results of a Bonferroni Post Hoc Test of Kruskal-Wallis were not observed between codes C and M, and between codes B and D.

We analysed the IRC measurements taken in the RBE for the buildings in the study area according to the simplified geological coding for the whole archipelago. From Fig. 4, we can see that geological codes A and C (acid rocks and clays) show different behaviour from the rest of the codes (B, D and M). The Bonferroni Post Hoc Test of Kruskal-Wallis does not show significant differences between codes C and A ($p - value = 0.37 > 0.05$), or between the pairs of codes B and D, B and M, and M and D ($p - value = 1.00 > 0.05$).

Table 5 shows that the IRC data measured for buildings in areas with geological codes A and C have geometric means of 134.3 Bq/m^3 and 180.2 Bq/m^3 respectively, corresponding to a high range of radon exposure (Table 3). In contrast, the IRC values for areas with geological codes B, D and M are very similar at around 60 Bq/m^3, corresponding to the low range of radon exposure (Table 3). This leads to a UTB for the IRC values in code A of 1021 Bq/m^3 (a factor of 3.4 higher than the RL of 300 Bq/m^3), whereas for code C, this value is 934 Bq/m^3 (a factor of 3.1 higher than the RL). For the rest of the geological codes, the UTBs are below the RL, as well as 90th percentile (P90). Hence, all statistical indicators confirm that codes B, D and M can be classified as low-risk geological areas, while codes A and C can be classified as high-risk geological areas.

5.2. Analysis of IRC data as a function of the TGR

For the analysis presented in this section, it was necessary to create a map using the inverse distance weighted interpolation (IDW) of the TGR data distributed throughout the study area, as shown in Fig. 5. For the IDW interpolation, a weighting coefficient of $P = 2$ and a pixel size of 100 × 100 m were used. This interpolated map allowed us to obtain TGR values corresponding to the locations in which the IRC measurements were made. Once the interpolated TGR values had been obtained for each IRC measurement location, they were grouped according to the ranges established by the CSN, as shown in Table 3.

Fig. 5 shows that the islands with the largest surface areas in the medium and high TGR ranges are Tenerife and Gran Canaria. For the rest of the islands, a large part of their surface area is in the low TGR range, with small nuclei in the medium and high ranges, approximately coinciding with areas of acid lithology (code A). However, in the southern half of La Palma, measurements were obtained in the medium/high range, as the predominant lithology corresponded to code B and, in a more dispersed way, code M. It should be noted that this region has undergone significant volcanic activity in recent years (Padrón et al., 2015), with a considerable increase after the Tajogaite eruption, with a flux of gases into the atmosphere such as CO_2 (Instituto Geográfico Nacional, 2023), which can be considered a carrier gas of ^{222}Rn (Elío et al., 2015; Etiope and Martinelli, 2002; Voltattorni et al., 2009). This phenomenon allows for a greater deposition of radon decay products on the surface, which may have influenced the gamma radiation measurements in this region.

Table 6
Statistical comparison of indoor radon concentration (IRC) results based on terrestrial gamma radiation (TGR) ranges.

	TGR < 7.5	7.5 < TGR < 14	TGR > 14
n	744	260	60
GM (Bq/m^3)	57.3	78.7	152.5
GSD (Bq/m^3)	2.5	3.1	3.6
UTB (Bq/m^3)	**198**	**389**	**1100**
P90 (Bq/m^3)	163	392	773

The box-and-whisker plot in Fig. 6 shows that the three groups have differentiated and staggered behaviour (as confirmed by the Bonferroni Post Hoc Test of Kruskal-Wallis, which indicates significant differences between each pair of ranges, $p - value = 0.00 < 0.05$). The lowest geometric mean for the IRC values (57.3 Bq/m^3) is found in the range of TGR values interpolated below 7.5 μR/h. Based on the ranges established by the CSN, these can be considered areas of low radon exposure (Table 3). From Table 6, we see that the medium and high TGR ranges have indicators that allow us to infer that these are areas with a high risk of exposure to radon, with a UTB for the IRC values of 389 Bq/m^3 in the medium range (a factor of 1.3 higher than the RL of 300 Bq/m^3) and 1100 Bq/m^3 in the high range (a factor of 3.7 higher than the RL).

5.3. Analysis of indoor radon concentration (IRC) data according to the level of risk based on geological information alone

In this section, we present an analysis of the IRC data in terms of risk levels based exclusively on lithostratigraphic features, for which risk maps of the Canary Islands were created based on geological information, following the methodology developed in previous work (Briones et al., 2023). As described in Section 6.1, the felsic lithologies corresponding to code A and the clayey lithologies corresponding to code C are areas of high radon risk, while the remaining codes B, D and M are areas of low risk (Fig. 2).

From the risk maps based on geology alone, we find that 54 % of the total IRC data points with values above 300 Bq/m^3 are located in the high-risk zone (Table 7). These high values account for 31 % of the total number of dwellings in this zone. In contrast, 90 % of the IRC values below 300 Bq/m^3 are located in the low-risk zone, representing 96 % of the total number of dwellings measured in this zone. In other words, only 4 % of the dwellings in the area that are classified as low-risk exceed the RL.

Fig. 7 shows a box-and-whisker plot of the IRC values categorised by risk level based on geological information. Differences can be observed between the group of IRC data in the low-risk zone and those corresponding to the high-risk zone, with geometric means of 57.5 Bq/m^3 and 151.8 Bq/m^3, respectively. From Table 7, it can be seen that the UTB values of the IRC measurements are 201 Bq/m^3 in low-risk areas (below the RL) and 917 Bq/m^3 in high-risk areas (approximately three times higher than the RL).

Table 7
Statistical comparison of indoor radon concentration (IRC) results based on risk levels for the three types of proposed radon risk maps.

	Risk map based on geological information		Risk map based on TGR		Combined Risk map	
	Low risk	High risk	Low risk	High risk	Low risk	High risk
n	922	142	744	320	700	364
n ($\geq 300\ Bq/m^3$)	37	44	26	55	16	65
n ($< 300\ Bq/m^3$)	885	98	718	265	684	299
GM (Bq/m^3)	57.5	151.8	57.3	89.1	54.2	94.2
GSD (Bq/m^3)	2.5	3.5	2.5	3.3	2.4	3.3
UTB (Bq/m^3)	**201**	**917**	**198**	**470**	**178**	**485**
P90 (Bq/m^3)	171	855	163	482	154	496

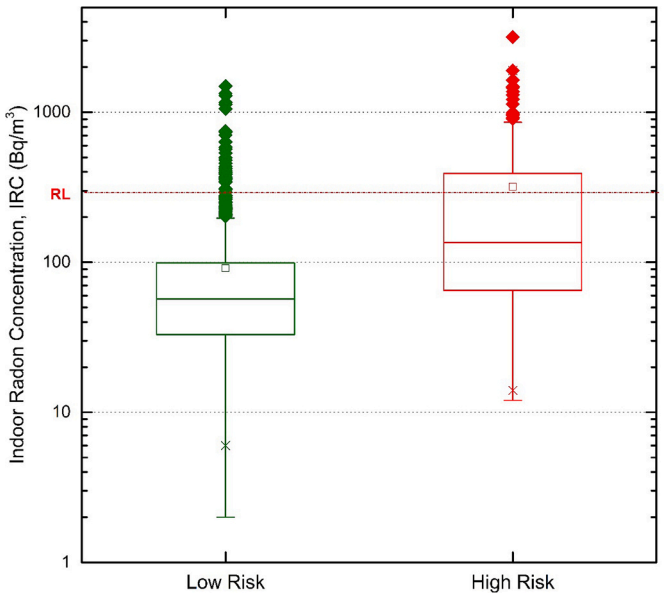

Fig. 7. Indoor Radon Concentration (IRC) data distributed by risk level based on geological information alone.

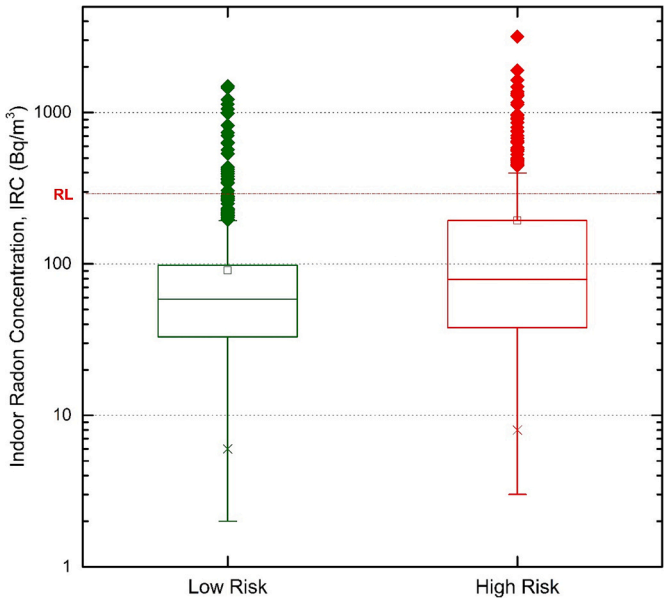

Fig. 8. Indoor Radon Concentration (IRC) data distributed by risk level based on Terrestrial Gamma Radiation (TGR) measurements alone.

5.4. Analysis of indoor radon concentration (IRC) data by level of risk based on terrestrial gamma radiation (TGR) measurements alone

This section presents an analysis of the IRC data categorised by risk level in the form of risk maps of the Canary Islands based exclusively on TGR measurements, with a classification level of 7.5 μR/h, as established in previous work (Briones et al., 2023). It should be noted that this level, which was established by the CSN, is considered a reliable indicator for the delimitation of priority areas for action against the risk of radon exposure (García-Talavera and López-Acevedo, 2019). Furthermore, from a statistical analysis of the IRC data against the ranges established by the CSN in Section 6.3, we see that the group of IRC values with an interpolated TGR of below 7.5 μR/h is the only one for which all the statistic indicators (geometric mean, UTB and P90) are within the limits for classification as a low-risk area, whereas the IRC values for the medium (between 7.5 μR/h and 14 μR/h) and high (above 14 μR/h) ranges indicate that these are high-risk areas.

Risk maps based solely on TGR measures lead to an increase in the area classified as high-risk. This is why this area contains 178 more data than the geological risk map (Table 7). In this case, 68 % of the total IRC data points above 300 Bq/m^3 are found to be in a high-risk area. In contrast, due to the aforementioned data transfer, 73 % of the total IRC values below 300 Bq/m^3 measured in the study area are located in the low-risk zone. However, if we restrict ourselves to the set of dwellings measured in the low-risk zone, we see that 97 % have an IRC below 300 Bq/m^3, meaning that only 3 % of the dwellings now have an IRC above the RL.

Fig. 8 shows a box-and-whisker plot of the IRC values. In the same way as for the maps based exclusively on geological information, a difference can be observed between the group of IRC data in the low-risk zone and those corresponding to high-risk areas, with geometric means of 57.3 Bq/m^3 and 89.1 Bq/m^3, respectively. Furthermore, as shown in Table 7, the UTB values of the IRC results in these zones are 198 Bq/m^3 (below the RL) and 470 Bq/m^3 (approximately 1.5 higher than the RL), respectively. These maps show a significant improvement in predictive capacity compared to those discussed in the previous section, and the IRC values measured for both risk zones give statistical results that confirm their suitability.

5.5. Risk mapping using a combination of geological information and terrestrial gamma radiation (TGR) measurements

When developing the methodology for radon risk mapping, it was found that certain high values of IRC in the study area could not be explained by the map based on geology alone, but could be represented by a map based on TGR measurements (Briones et al., 2023). This is due to the fact that certain areas with mainly basic lithologies (code B) show different radiological behaviour from most code B lithologies. This means that we can define a risk map by combining these two types of map.

Fig. 9 shows combined risk maps of the Canary Islands created using this methodology, where the coloured urban grid indicates the corresponding risk level.

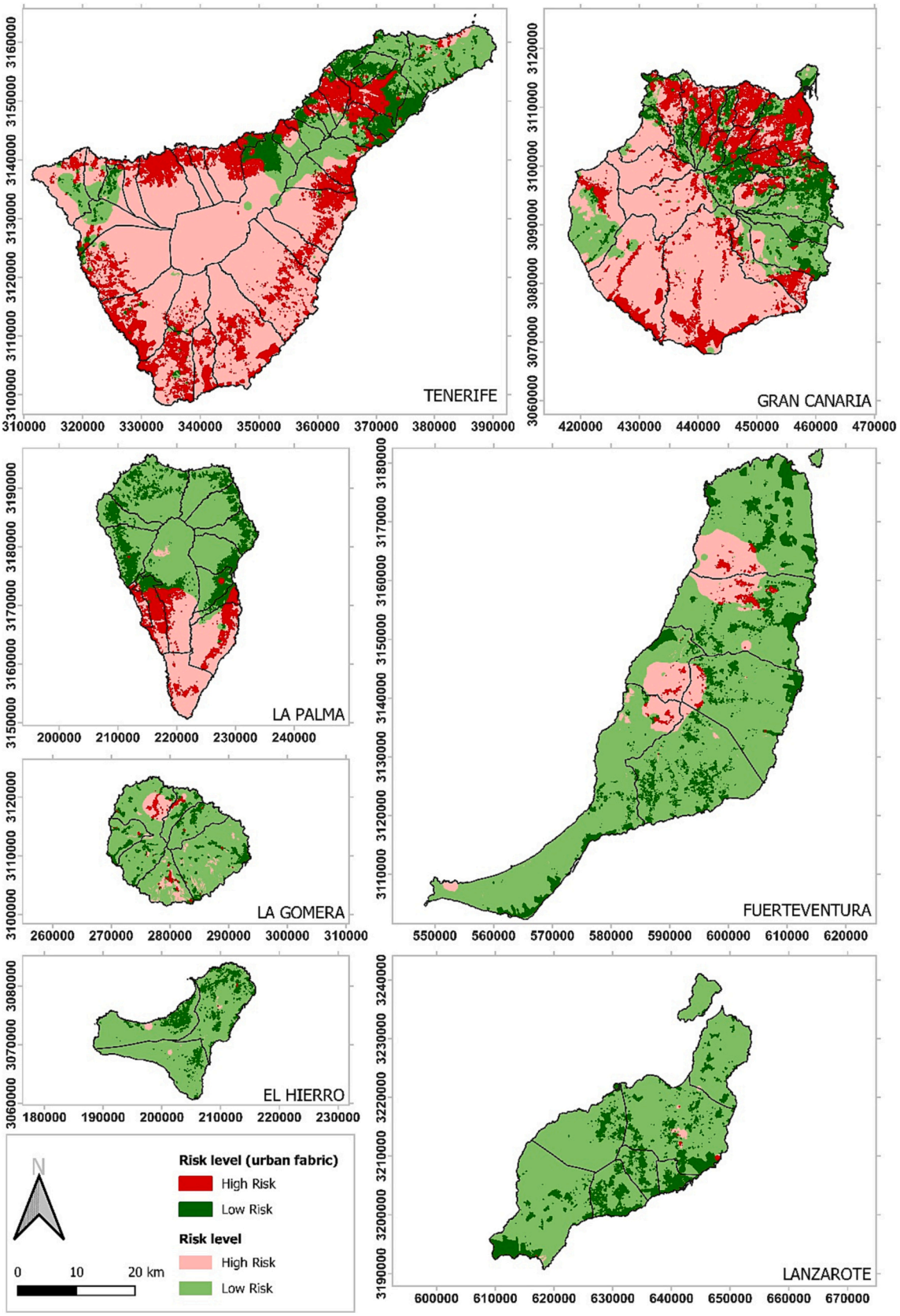

Fig. 9. Combined risk maps based on geological information and Terrestrial Gamma Radiation data of Canary Islands with the urban fabric highlighted.

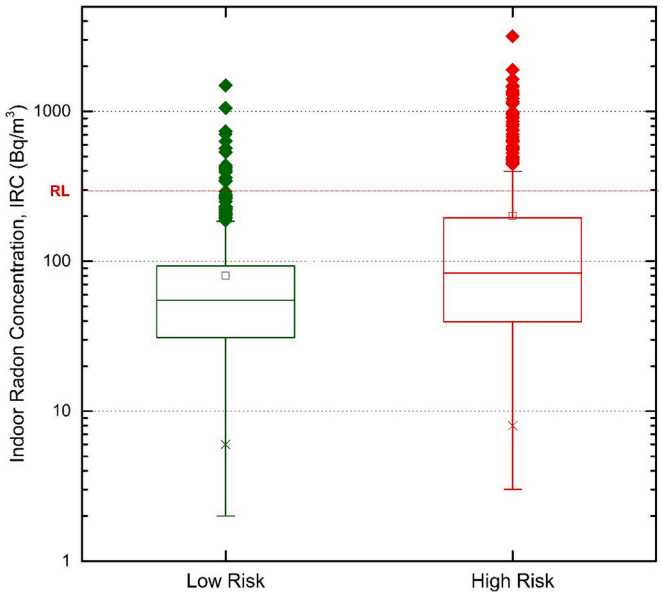

Fig. 10. Indoor Radon Concentration (IRC) data distributed by combined risk level.

When these combined risk maps based on geology and TGR measurements are analysed, we see a further increase in the area classified as high risk. In this case, 44 more data points are lay in this area (Table 7), meaning that 80 % of the total IRC values above 300 Bq/m^3 are now in the high-risk zone. In contrast, due to this slight shift in data, 70 % of the IRC values below 300 Bq/m^3 are in the low-risk zone. However, as in the previous case, if we restrict ourselves to the set of dwellings measured in the low-risk zone, 98 % have an IRC below 300 Bq/m^3, and only 2 % have an IRC above the RL.

Fig. 10 shows a box-and-whisker plot of the IRC data. A difference can be observed between the IRC datasets for low-risk and high-risk areas, with geometric means of 54.2 Bq/m^3 and 94.2 Bq/m^3, respectively. This was confirmed by a Mann-Whitney *U* test, which indicated significant differences between the two groups with a $p - value = 0.00 < 0.05$. Furthermore, as shown in Table 7, the UTB values for the IRC data in these areas are 178 Bq/m^3 (below the RL) and 485 Bq/m^3 (62% above the RL), respectively.

Of the three formats described above, the combined map gives the highest percentage of IRC data above the RL in areas classified as high-risk, while considerably minimising the number of high IRC cases in areas classified as low-risk. It is worth noting the conservative nature of this map, as the increased area classified not only brings together high values, but also a greater number of measurements with low IRC. However, the use of this map gives a low-risk area with stronger confidence by minimising the number of high IRC data. In addition, the UTB of the IRC values in this zone is 41 % lower than the RL, the lowest of all three types of risk map.

5.6. Delimitation of risk zones based on urban fabric

With the aim of achieving a better approximation that implies the consideration of these risk levels in the different population areas of the Canary Islands, the combined risk maps for the islands were cross-referenced with the urban fabric map, which shows plots used for residential, commercial and industrial purposes, as well as those areas that could be built on or which are undergoing urbanisation. The highlighted plot according to the corresponding level of risk is shown in Fig. 9.

One of the zoning strategies used as a basis for priority action

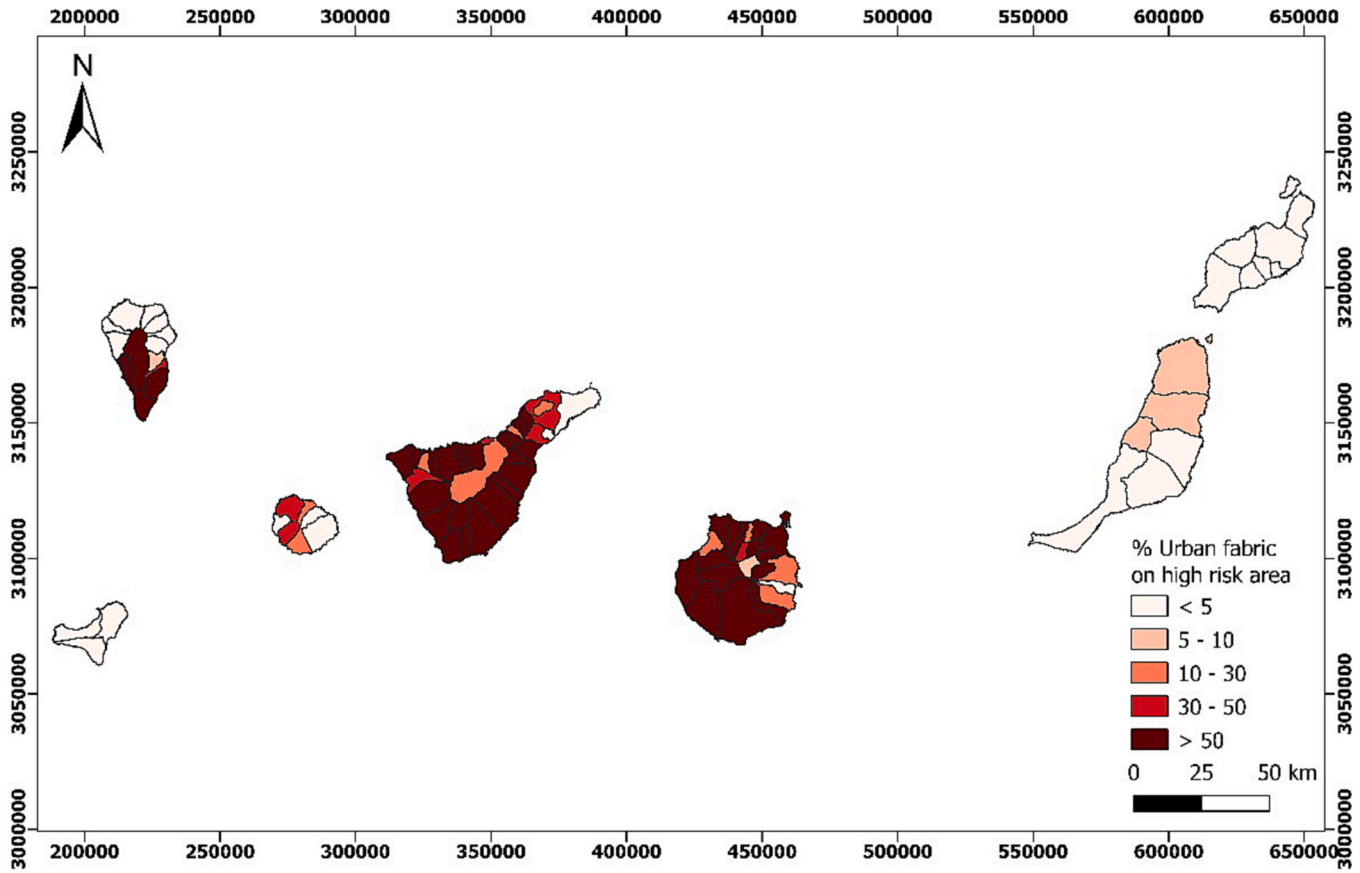

Fig. 11. Municipality zoning based on the percentage of urban fabric on high-risk area.

measures by the authorities is the delimitation of zones by administrative regions. A potential zoning method could be based on cross-referencing between the urban fabric and the radon risk map, which would make it possible to assess the extent of the risk of radon exposure affecting the building stock of each municipality, based on the percentage of urban fabric affected by the high-risk areas in relation to the urban fabric as a whole (García-Talavera and López-Acevedo, 2019).

In view of the above discussion, Fig. 11 presents a municipal zoning map of the Canary Islands based on the percentage of urban fabric falling into areas classified as high-risk according to the combined risk map. Of the 88 municipalities, 27 have <10 % of their urban fabric in high-risk zones, and of these, 22 have between zero and 5 % of their urban fabric in high-risk zones. In contrast, 41 municipalities have more than half of their urban fabric in a high-risk zone.

5.7. *Effective dose to the population in risk areas*

Using the risk maps created in this study, we can calculate the effective dose received by a worker within a workplace according to the risk area in which the building is located, and an exposure time of 2000 h (corresponding to 50 weeks of 40 h of work) was estimated.

When we take these considerations into account and take the UTB obtained in each of the zones established in the risk maps as the radon concentration value, we can estimate with 90 % probability that 90 % of the working population whose workplace is located in a low-risk zone will receive an annual dose of ≤2.46 mSv/year. However, this value rises to 6.70 mSv/year for workplaces in areas classified as high-risk according to the combined risk map. Nevertheless, it should be made clear that the maps and dose calculations may give some overall estimates, but in no case is it an individual dose calculation, which it should be based on direct measurements. This value exceeds the limit set out in the current national regulations of 6 mSv/year for the annual effective to a worker dose due to radon (Ministerio de la Presidencia and R. con las C. y M.D, 2022), above which radiological protection measures must be implemented. This supports our findings of the alignment between the combined risk maps and the conditions foreseen for those cases located in the risk zone within the current regulations.

6. Conclusions

This paper has presented a new radon risk mapping of the Canary Islands based on a combination of lithostratigraphic information regarding the soils on which the buildings are located and high-resolution terrestrial gamma radiation maps. These risk maps were obtained by applying a methodology that was developed previously by our team when working in a smaller study area formed of different representative municipalities of the Canary Islands, and by extending it to the whole archipelago.

1) In order to simplify the available lithostratigraphic information, a simplified coding of the rocks and soils of the Canary Islands was used. A statistical analysis of the IRC data showed that acidic and clayey soils (codes A and C) are prone to radon emission, and could therefore be classified as high-risk areas. In contrast, statistical results for basic (code B), deposits (code D) and mixed (code M) soils confirmed that they could be classified as low-risk areas.
2) By applying the TGR ranges established by the CSN limits to the interpolated map of TGR measurements, it was verified that the UTB for IRC data measured in areas with a lower TGR range (<7.5 μR/h) was lower than 300 Bq/m^3, whereas the middle (between 7.5 and 14 μR/h) and upper (≥ 14 μR/h) ranges had a UTB above the RL, meaning that that the areas with middle and high TGR ranges could be classified as high-risk areas.
3) While the risk maps based solely on geological information and those based solely on TGR measurements were able to delimit the most radon-prone areas with a high level of efficiency, the maps obtained by combining both of these were able to indicate the highest number of cases of dwellings with a IRC higher than 300 Bq/m^3 in areas classified as high-risk, while in areas classified as low-risk, only 2 % of the dwellings studied had a IRC higher than 300 Bq/m^3.
4) The combined risk map has a conservative character, as merging maps based on geology and TGR measurements allows the surface area classified as high-risk to be increased. This means that the map is capable of bringing together a greater number of dwellings within these zones, not only including cases where the IRC is high, but also dwellings with values lower than the RL. However, this allows the combined map to provide a greater margin of safety, since the UTB of the IRC values of the dwellings located in low-risk areas is 41 % lower than the RL, a lower value than for the non-combined risk maps.
5) Cross-referencing the risk map with the urban fabric map made it possible to better distinguish the effects on the population in areas classified as high-risk. A municipal zoning map was produced in which 27 of the 88 municipalities in the Canary Islands had <10 % of their urban fabric in a high-risk area.
6) By applying a dosimetric model, it was possible to perform an estimation of the overall annual effective dose received by a worker in a low-risk area. It was estimated to be lower than 2.46 mSv/year, whereas in high-risk areas this estimation rises to 6.70 mSv/year, higher than the limit of 6 mSv/year established by the current regulations.

CRediT authorship contribution statement

C. Briones: Writing – review & editing, Writing – original draft, Visualization, Validation, Methodology, Investigation, Data curation. **J. Jubera:** Supervision, Project administration, Methodology, Investigation, Data curation. **H. Alonso:** Resources, Project administration, Methodology, Investigation. **J. Olaiz:** Resources, Project administration, Investigation. **J.T. Santana:** Resources, Investigation. **N. Rodríguez-Brito:** Resources, Investigation. **A.C. Arriola-Velásquez:** Visualization, Investigation, Data curation. **N. Miquel:** Visualization, Investigation, Data curation. **A. Tejera:** Resources, Investigation. **P. Martel:** Resources, Investigation, Data curation. **E. González-Díaz:** Writing – review & editing, Supervision, Formal analysis, Data curation. **J.G. Rubiano:** Writing – review & editing, Supervision, Project administration, Methodology, Investigation.

Declaration of competing interest

The authors declare that they have no known competing financial interests or personal relationships that could have appeared to influence the work reported in this paper.

Data availability

The data that has been used is confidential.

Acknowledgements

This work was financed by Government of the Canary Islands (Consejería de obras públicas, transporte y vivienda) through the collaboration agreement with the University of Las Palmas de Gran Canaria for a “Proposal for a newzoning to predict the level of risk derived from the presence of radon concentrations inside buildings”. Some data was partially supported by the Spanish Nuclear Safety Council through a grant of its R&D programme 2012. The lithostratigraphic maps were obtained from Cartografía Digital del Mapa Geológico y Continuo de España (GEODE) supplied by Instituto Geológico y Minero de España (IGME).

References

Alonso, H.E., 2015. El radón en Suelos, Rocas, Materiales de construcción Y Aguas subterráneas de Las Islas Canarias Orientales (Radon in Soils, Rocks, Construction Materials and Groundwater of the Eastern Canary Islands) [PhD Dissertation].. Universidad de Las Palmas de Gran Canaria.

Alonso, H., Rubiano, J.G., Guerra, J.G., Arnedo, M.A., Tejera, A., Martel, P., 2019. Assessment of radon risk areas in the Eastern Canary Islands using soil radon gas concentration and gas permeability of soils. Sci. Total Environ. 664, 449–460. https://doi.org/10.1016/j.scitotenv.2019.01.411.

Arnedo, M.A., 2014. Evaluación del Fondo Radiactivo Natural de Las Islas Canarias Orientales, Implicaciones radiológicas Sobre la población (Evaluation of the Natural Radioactive Background of the Eastern Canary Islands, Radiological Implications on the Population) [PhD Dissertation].. Universidad de Las Palmas de Gran Canaria.

Arnedo, M.A., Rubiano, J.G., Alonso, H., Tejera, A., González, A., González, J., Gil, J.M., Rodríguez, R., Martel, P., Bolivar, J.P., 2017. Mapping natural radioactivity of soils in the eastern Canary Islands. J. Environ. Radioact. 166, 242–258. https://doi.org/10.1016/j.jenvrad.2016.07.010.

Barbosa, S., Huisman, J.A., Azevedo, E.B., 2018. Meteorological and soil surface effects in gamma radiation time series - implications for assessment of earthquake precursors. J. Environ. Radioact. 195, 72–78. https://doi.org/10.1016/j.jenvrad.2018.09.022.

Bouville, A., Lowder, W.M., 1988. Human population exposure to cosmic radiation. Radiat. Prot. Dosim. 24, 293–299. https://doi.org/10.1093/oxfordjournals.rpd.a080290.

Briones, C., Jubera, J., Alonso, H., Olaiz, J., Santana, J.T., Rodríguez-Brito, N., Tejera, A., Martel, P., González-Díaz, E., Rubiano, J.G., 2021. Methodology for determination of radon prone areas combining the definition of a representative building enclosure and measurements of terrestrial gamma radiation. Sci. Total Environ. 788, 147709 https://doi.org/10.1016/j.scitotenv.2021.147709.

Briones, C., Jubera, J., Alonso, H., Olaiz, J., Santana, J.T., Rodríguez-Brito, N., Arriola-Velásquez, A.C., Miquel, N., Tejera, A., Martel, P., González-Díaz, E., Rubiano, J.G., 2023. Multiparametric analysis for the determination of radon potential areas in buildings on different soils of volcanic origin. Sci. Total Environ. 885, 163761 https://doi.org/10.1016/j.scitotenv.2023.163761.

Carracedo, J.C., Pérez Torrado, F.J., Ancochea, E., Meco, J., Hernán, F., Cubas, C.R., Casillas, R., Rodríguez-Badiola, E., Ahijado, A., 2002. Cenozoic Volcanism II: the Canary Islands., in: The Geological Society London.

Cinelli, G., Tondeur, F., Dehandschutter, B., 2011. Development of an indoor radon risk map of the Walloon region of Belgium, integrating geological information. Environ. Earth Sci. 62, 809–819. https://doi.org/10.1007/s12665-010-0568-5.

Cinelli, G., De Cort, M., Tollefsen, T., 2019. European Atlas of Natural Radiation. Publication Office of the European Union, Luxembourg.

Collignan, B., Le Ponner, E., Mandin, C., 2016. Relationships between indoor radon concentrations, thermal retrofit and dwelling characteristics. J. Environ. Radioact. 165, 124–130. https://doi.org/10.1016/j.jenvrad.2016.09.013.

Consejo de Seguridad Nuclear, 2012. Guía de Seguridad 11.4. Metodología para la evaluación de la exposición al radón en los lugares de trabajo (Safety Guide 11.4. Methodology for evaluating radon exposure in workplaces). Collect. CSN Secur. Guid.

Elío, J., Ortega, M.F., Nisi, B., Mazadiego, L.F., Vaselli, O., Caballero, J., Grandia, F., 2015. CO2 and Rn degassing from the natural analog of Campo de Calatrava (Spain): implications for monitoring of CO2 storage sites. Int. J. Greenh. Gas Control 32, 1–14. https://doi.org/10.1016/j.ijggc.2014.10.014.

Elío, J., Crowley, Q., Scanlon, R., Hodgson, J., Long, S., 2017. Logistic regression model for detecting radon prone areas in Ireland. Sci. Total Environ. 599–600, 1317–1329. https://doi.org/10.1016/j.scitotenv.2017.05.071.

Etiope, G., Martinelli, G., 2002. Migration of carrier and trace gases in the geosphere: an overview. Phys. Earth Planet. Inter. 129, 185–204. https://doi.org/10.1016/S0031-9201(01)00292-8.

Euratom, B.S.S., 2014. Council Directive 2013/59/Euratom of 5 December 2013 laying down basic safety standards for protection against the dangers arising from exposure to ionising radiation, and repealing Directives 89/618/Euratom, 90/641/Euratom, 96/29/Euratom, 97/43/Euratom a 1–73.

Fernández, A., Sainz, C., Celaya, S., Quindós, L., Rábago, D., Fuente, I., 2021. A new methodology for defining radon priority areas in Spain. Int. J. Environ. Res. Public Health 18, 1–16. https://doi.org/10.3390/ijerph18031352.

Font, L., 1997. Radon Generation, Entry and Accumulation Indoors [PhD Dissertation].. Universidad Autónoma de Barcelona.

García-Talavera, M., López-Acevedo, F.J., 2019. Cartografía del potencial de radón de España (Mapping Spain's radon potential). Colección Inf. Técnicos del Cons. Segur, Nucl.

García-Talavera, M., García-Pérez, A., Rey, C., Ramos, L., 2013. Mapping radon-prone areas using γ-radiation dose rate and geological information. J. Radiol. Prot. 33, 605–620. https://doi.org/10.1088/0952-4746/33/3/605.

Herranz, M., Jiménez, R., Navarro, E., Payeras, J., Pinilla, J.L., 2003. Procedimiento de toma de muestras para la determinación de radioactividad en suelos capa superficial (Sampling procedure for determining radioactivity in soil surface layer). Colección Inf. Técnicos 11 (2003), 15.

Hughes, M.B., Elío, J., Crowley, Q.G., 2022. A user's guide to radon priority areas, examples from Ireland. J. Eur. Radon Assoc. 1–12 https://doi.org/10.35815/radon.v3.7586.

ICRP, 2010. Lung Cancer Risk from Radon and Progeny and Statement on Radon. ICRP Publication 115, Ann. ICRP 40(1). Prot. Int. Comm. Radiol. 6, 1. doi:https://doi.org/10.1016/0146-6453(81)90127-5.

ICRP, 2014. Radiological protection against radon exposure. ICRP Publication 126. Ann. ICRP 43(3)., Protection, International Commission on Radiological.

Ielsch, G., Cushing, M.E., Combes, P., Cuney, M., 2010. Mapping of the geogenic radon potential in France to improve radon risk management: methodology and first application to region Bourgogne. J. Environ. Radioact. 101, 813–820. https://doi.org/10.1016/j.jenvrad.2010.04.006.

IGME, 2021. Cartografía Digital del Mapa Geológico Y Continuo de España GEODE (Comunidad Autónoma de Canarias) (Digital Cartography of the Geological and Continuous Map of Spain GEODE (Canary Islands)). Inst. Geológico y Min, España.

IGME, 2022. IC6031 File in the Spanish Inventory of Geological Sites of Interest.

Instituto Geográfico Nacional, 2023. Gas report 09/27/2023 Earthquake - volcanic series 09 11 2021, Cumbre Vieja, La Palma [WWW Document]. URL https://volcan.lapalma.es/documents/57f1b0010bc34dc3a17ee4c0ea3ddcbd/explore.

ISTAC, 2009. Edificios según número de Plantas Sobre Rasante (Buildings According to Number of Floors above Ground) (Datos Abiertos del Instituto Canario de Estadística del Gobierno de Canarias).

Kropat, G., Bochud, F., Jaboyedoff, M., Laedermann, J.P., Murith, C., Palacios, M., Baechler, S., 2014. Major influencing factors of indoor radon concentrations in Switzerland. J. Environ. Radioact. 129, 7–22. https://doi.org/10.1016/j.jenvrad.2013.11.010.

Le Maitre, R.W., 2002. Igneous rock. A classification and glossary of terms. In: Recommendations of the International Union of Geological Sciences Subcommission on the Systematics of Igneous Rocks. Cambridge University Press. https://doi.org/10.1017/CBO9781107415324.004.

McColl, N.P., Bradley, E.J., Gooding, T.D., Ashby, C., Astbury, J., Akinson, J., Harrall, R., Howard, T., Hunt, J., Kernohan, D., James, K., Jones, R., Laverty, J., McMahon, N., McNicholas, C., Moss, L., Murphy, L., Netherwood, T., Rankin, P., Stewart, M., Taylor, J., Tink, V., Waldron, G., Wasson, G., 2018. UK National Radon Action Plan About Public Health England. Public Heal, England.

Meeker, W.Q., Hahn, G.J., Escobar, L.A., 1991. Statistical Intervals: A Guide for Practitioners. Wiley, p. cop.

Miles, J.C.H., Appleton, J.D., Rees, D.M., Adlam, K.A.M., Scheib, C., Myers, A.H., Green, B.M.R., Mccoll, N.P., 2011. Indicative atlas of radon in Scotland (report HPA-CRCE-023). Public Heal. Engl. 1–33.

Ministerio de Fomento, 2019. Documento Básico de Salubridad HS, Sección HS 6 Protección frente a la exposición de radón (HS Basic Health Standards Document, Section 6, Protection against radon exposure). Boletín Of. del Estado 2013, 1–129.

Ministerio de la Presidencia, R. con las C. y M.D., 2022. Real Decreto 1029/2022, de 20 de diciembre, por el que se aprueba el Reglamento sobre protección de la salud contra los riesgos derivados de la exposición a las radiaciones ionizantes. (Royal Decree 1029/2022, of December 20, which approves the Regulation on health protection against the risks derived from exposure to ionizing radiation). Boletín Of. del Estado.

Odeh, R.E., Owen, D.B., 1980. Tables for Normal Tolerance Limits, Sampling Plans, and Screening.

Padrón, E., Pérez, N.M., Rodríguez, F., Melián, G., Hernández, P.A., Sumino, H., Padilla, G., Barrancos, J., Dionis, S., Notsu, K., Calvo, D., 2015. Dynamics of diffuse carbon dioxide emissions from Cumbre Vieja volcano, La Palma. Canary Islands. Bull. Volcanol. 77 https://doi.org/10.1007/s00445-015-0914-2.

Pereira, A., Lamas, R., Miranda, M., Domingos, F., Neves, L., Ferreira, N., Costa, L., 2017. Estimation of the radon production rate in granite rocks and evaluation of the implications for geogenic radon potential maps: a case study in Central Portugal. J. Environ. Radioact. 166, 270–277. https://doi.org/10.1016/j.jenvrad.2016.08.022.

Quindós Poncela, L.S., Fernández, P.L., Gómez Arozamena, J., Sainz, C., Fernández, J.A., Suarez Mahou, E., Martin Matarranz, J.L., Cascón, M.C., 2004. Natural gamma radiation map (MARNA) and indoor radon levels in Spain. Environ. Int. 29, 1091–1096. https://doi.org/10.1016/S0160-4120(03)00102-8.

Suárez-Mahou, E., Fernández-Amigot, Á., Moro, M., García-Pomar, D., Moreno, J., Lanaja, J., 2000. Proyecto Marna. Mapa de radiación gamma natural, INT-04-02 (Marna Project. Natural gamma radiation map, INT-04-02). Colección Inf. Técnicos Cons. Segur. Nucl.

Tondeur, F., Cinelli, G., 2014. A software for indoor radon risk mapping based on geology. Nucl. Technol. Radiat. Prot. 29, 59–63. https://doi.org/10.2298/NTRP140SS59T.

Troll, V.R., Carracedo, J.C., 2016a. The Geology of El Hierro, The Geology of the Canary Islands. Elsevier Inc. https://doi.org/10.1016/b978-0-12-809663-5.00002-5

Troll, V.R., Carracedo, J.C., 2016b. The Geology of La Palma, The Geology of the Canary Islands. Elsevier Inc. https://doi.org/10.1016/b978-0-12-809663-5.00003-7

Troll, V.R., Carracedo, J.C., 2016c. The Geology of La Gomera, The Geology of the Canary Islands. Elsevier Inc. https://doi.org/10.1016/b978-0-12-809663-5.00004-9

Troll, V.R., Carracedo, J.C., 2016d. The Geology of Tenerife, The Geology of the Canary Islands. Elsevier Inc. https://doi.org/10.1016/b978-0-12-809663-5.00005-0

Troll, V.R., Carracedo, J.C., 2016e. The Geology of Gran Canaria, The Geology of the Canary Islands. Elsevier Inc. https://doi.org/10.1016/b978-0-12-809663-5.00006-2

Troll, V.R., Carracedo, J.C., 2016f. The Geology of Fuerteventura, The Geology of the Canary Islands. Elsevier Inc. https://doi.org/10.1016/b978-0-12-809663-5.00008-6

Troll, V.R., Carracedo, J.C., 2016g. The Geology of Lanzarote, The Geology of the Canary Islands. Elsevier Inc. https://doi.org/10.1016/b978-0-12-809663-5.00007-4

UNSCEAR, 1993. Sources and Effects of Ionazing Radiation, in: J. Radiological Protection, Annex IV.

UNSCEAR, 2000. Sources and Effects of Ionizing Radiation. United Nations Scientific Committee on the Effects of Atomic Radiation, United Nations, New York.

UNSCEAR, 2008. Report on Sources and Effects of Ionizing Radiation., United Nations Scientific Committee on the Effects of Atomic Radiation. United Nations, New York.

Voltattorni, N., Sciarra, A., Caramanna, G., Cinti, D., Pizzino, L., Quattrocchi, F., 2009. Gas geochemistry of natural analogues for the studies of geological CO2 sequestration. Appl. Geochem. 24, 1339–1346. https://doi.org/10.1016/j.apgeochem.2009.04.026.

World Health Organization, 2009. WHO Handbook on Indoor Radon. A Public Health Perspective.

Zafrir, H., Barbosa, S.M., Malik, U., 2013. Differentiation between the effect of temperature and pressure on radon within the subsurface geological media. Radiat. Meas. 49, 39–56. https://doi.org/10.1016/j.radmeas.2012.11.019.